

EULERIAN-LAGRANGIAN METHODOLOGY APPLIED IN THE SOLUTION OF FLOW IN TRIANGULAR CAVITY

Bruno Manoel Pasquim¹, bpasquim@hotmail.com

Viviana Cocco Mariani², viviana.mariani@pucpr.br

¹Programa de Graduação em Engenharia Química, Pontifícia Universidade Católica do Paraná

²Programa de Pós-Graduação em Engenharia Mecânica, Pontifícia Universidade Católica do Paraná

Rua Imaculada Conceição, 1155, CEP: 80215-901, Curitiba - PR - Brasil

Abstract. *This study presents the Eulerian-Lagrangian methodology and its application to solve a steady flow in a lid-driven triangular two-dimensional cavity. The evolution of the velocities, stream function, and vorticity inside a triangular lid-driven cavity, when the Reynolds number changes of 1 to 6000, is presented. For space discretization inside of triangular cavity the orthogonal Cartesian's mesh is used. Then, using this mesh, trapezoidal volumes appear in the interface between solid and fluid. For a suitable treatment of these volumes the Eulerian-Lagrangian methodology is used. The Navier-Stokes equations are solved numerically using finite-volume method and the algebraic equations system is solved by an iterative method. Results show the development of new eddies with increasing of Reynolds number. It is observed also that the interior of the primary eddy has almost constant stream function and vorticity for reasonably large Reynolds number. Some results for the triangular cavity problem are compared with results in the literature and the agreement is good.*

Keywords: *Triangular Cavity, Lid-Driven Cavity, Eulerian-Lagrangian Method, Finite-Volume Method.*

1. INTRODUCTION

The incompressible flow of a fluid in lid-driven cavities is a problem of primary importance in computational fluid dynamics, the development of improved methods to solve these problems has also been a subject of concern to computational physicists for many years. The results for the square cavities may not be applied to other important geometries such as trapezoidal or triangular cavities. In irregular cavities special attention has been given to boundaries, i.e., for example, the classic finite-volume method, using structured meshes, should be changed to solve the flow in these geometries. These differences promote the development of the searches and of new numerical methods each time more fast and accurate for the solution of flows in irregular geometries. Related to present study can emphasize the following works.

There have, a few studies of flow in curved and nonrectangular geometries. Vynnycky and Kimura (1994) reported the results of their study of steady flow in a driven quarter circular cavity. Ribbens et al. (1991) described the flow in an elliptic region with a moving boundary. The flow in a trapezoidal cavity was studied by Darr and Vanka (1991). Although curved and nonrectangular geometries may be represented using curvilinear and non orthogonal structured grids, thus triangular cavities can be used to test new numerical methods. Some of the problems encountered have been explained in detail by Ribbens et al. (1994). The triangular cavity also exhibits interesting flow features that have been analytically studied by Moffat (1963) in the Stokes regime and by Batchelor (1956) to upper Reynolds number.

Li and Tang (1996) studied the flow in equilateral triangular cavities, described that the flow features is highly stable as a square cavity, besides verified the independence of primary eddy position with the Reynolds number (Re) and has shown that the interior region attains constant vorticity with the increasing of Reynolds number. Other model of triangular cavity was studied by Jyotsna and Vanka (1995), with various eddies inside the cavity. The cavity had a height larger than width. The most important feature of the flow was the occurrence of an infinite sequence of eddies of decreasing size and rapidly decreasing intensity towards the stationary corner. In semi-circular cavities when Reynolds number increases the primary eddy changes the position in direction to top of lid-driven cavity as verified by Glowinski et al. (2006).

The main goal of this article is to investigate the capability of Eulerian-Lagrangian method to solve the steady flow in a triangular cavity that has inclined boundaries. The paper is organized as follows. Section 2 introduces the formulation of the problem and shows the space discretization of governing equations. Numerical results are presented in Section 3, including a comparison with some numerical results presented in Li and Tang (1996) and McQuain et al. (1994). Streamlines and contours of vorticity are presented to $Re \leq 6000$ in the same section.

2. PROBLEM FORMULATION

Figure 1 shows the geometry of the triangular cavity, with the coordinate system used here. In the flow region, is solved the Navier-Stokes equations governing a two-dimensional, steady, incompressible flow of constant fluid properties. These equations are written in primitive variables (u , v , and p) as (Fox e McDonald, 2001),

$$\frac{\partial u}{\partial x} + \frac{\partial v}{\partial y} = 0, \quad (1)$$

$$\frac{\partial(uu)}{\partial x} + \frac{\partial(vu)}{\partial y} = -\frac{\partial p}{\partial x} + \nu \left[\frac{\partial^2 u}{\partial x^2} + \frac{\partial^2 u}{\partial y^2} \right], \quad (2)$$

$$\frac{\partial(uv)}{\partial x} + \frac{\partial(vv)}{\partial y} = -\frac{\partial p}{\partial y} + \nu \left[\frac{\partial^2 v}{\partial x^2} + \frac{\partial^2 v}{\partial y^2} \right], \quad (3)$$

where u (m/s) and v (m/s) are the velocity components in the x and y directions, respectively, ν (m²/s) e ρ (kg/m³) are the dynamics viscosity and density, respectively, and p (Pa) is the a pressure.

The boundary conditions for triangular cavity, in Fig. 1, are given as follows:

- (i) $u = 1, v = 0$ for $y = H$ and $0 \leq x \leq L$;
- (ii) $u = 0, v = 0$ for $y = f(x) = -\sqrt{3}x + 3$ and $0 \leq x \leq L/2$.
- (iii) $u = 0, v = 0$ for $y = f(x) = \sqrt{3}x - 3$ and $L/2 < x \leq L$.

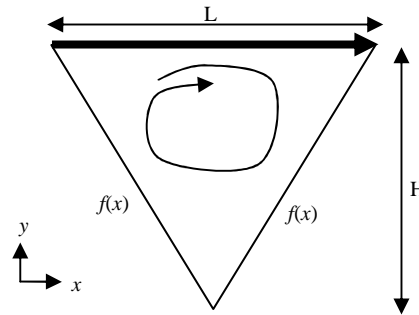


Figure 1. Triangular cavity.

The lid-driven cavity depicted in Fig. 1 has the dimensions $L = 2\sqrt{3}$ m and $H = 3$ m, generating an equilateral cavity with length of each side $2\sqrt{3}$ m.

As a common practice Eqs. (1) to (3) can be expressed by a single equation for the generic variable ϕ as

$$\frac{\partial(\rho u \phi)}{\partial x} + \frac{\partial(\rho v \phi)}{\partial y} = \Gamma^\phi \frac{\partial}{\partial x} \left(\frac{\partial \phi}{\partial x} \right) + \Gamma^\phi \frac{\partial}{\partial y} \left(\frac{\partial \phi}{\partial y} \right) + S^\phi. \quad (4)$$

where ϕ is equal to u and v for Eqs. (2) and (3), respectively, and equal to unity for Eq. (1), and Γ^ϕ and S^ϕ are, respectively, the diffusion coefficient and term source. The governing equation, Eq. (4), will be discretized first in the full cells and following the discretization is presented for trapezoidal cells in the boundaries.

2.1. Discretization for full volumes

The Eq. (4) with their respective boundary conditions is solved in this work using the finite-volume method described by Patankar (1980). The cavity is divided into small no overlapping rectangular control volumes. The co-localized arrangement is utilized, i.e., in the center of each control volume is located a nodal point where are stored all interesting variables. Integrating the Eq. (4) over a typical control volume in the fluid domain, such as the one presented in Fig. 2, yields,

$$\int_s^e \int_w^n \frac{\partial(\rho u \phi)}{\partial x} dx dy + \int_w^e \int_s^n \frac{\partial(\rho v \phi)}{\partial y} dy dx = \int_s^e \int_w^n \Gamma^\phi \frac{\partial^2 \phi}{\partial x^2} dx dy + \int_w^e \int_s^n \Gamma^\phi \frac{\partial^2 \phi}{\partial y^2} dy dx + \bar{S}^\phi, \quad (5)$$

where subscripts e, w, n and s denote the faces east, west, north, and south of the control volume, respectively, as shown in Fig. 2, and \bar{S}^ϕ is the average value of term source.

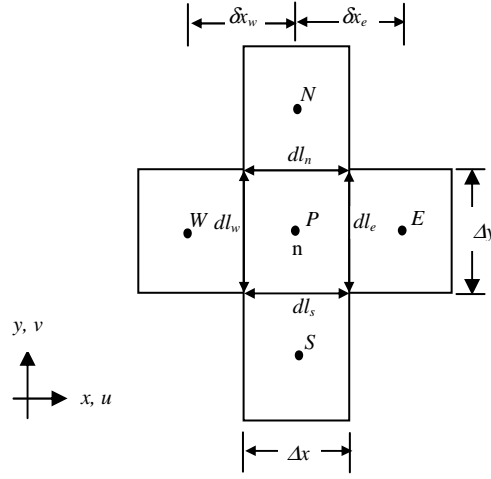


Figure 2. Typical control volume.

The Eq. (5) can be rewritten as,

$$(\rho u \phi dl)_e - (\rho u \phi dl)_w + (\rho v \phi dl)_n - (\rho v \phi dl)_s = \bar{S}^\phi + \Gamma_e^\phi \frac{\partial \phi}{\partial x} dl_e - \Gamma_w^\phi \frac{\partial \phi}{\partial x} dl_w + \Gamma_n^\phi \frac{\partial \phi}{\partial y} dl_n - \Gamma_s^\phi \frac{\partial \phi}{\partial y} dl_s. \quad (6)$$

Substituting convective and total fluxes represented by $F = (\rho \mathbf{u} dl)$ and $J = [\rho \mathbf{u} \phi - \Gamma^\phi (\partial \phi / \partial \mathbf{n})] dl$, respectively, in Eq. (6) and subtracting from the resulting equation the equation of mass conservation multiplied by ϕ_P results, after some adjustments, in

$$(J_e - F_e \phi_P) - (J_w - F_w \phi_P) + (J_n - F_n \phi_P) - (J_s - F_s \phi_P) = \bar{S}^\phi. \quad (7)$$

Thus, the algebraic equation for the control volume P can be expressed as

$$\begin{aligned} a_P \phi_P &= a_E \phi_E + a_W \phi_W + a_N \phi_N + a_S \phi_S + \bar{S}^\phi, \\ a_E &= D_e A |P_e| + \langle -F_e, 0 \rangle, \\ a_W &= D_w A |P_w| + \langle F_w, 0 \rangle, \\ a_N &= D_n A |P_n| + \langle -F_n, 0 \rangle, \\ a_S &= D_s A |P_s| + \langle F_s, 0 \rangle, \\ a_P &= a_E + a_W + a_N + a_S, \\ \bar{S}^\phi &= \begin{cases} -p_e dl_e + p_w dl_w, & \text{if } \phi = u, \\ -p_n dl_n + p_s dl_s, & \text{if } \phi = v. \end{cases} \end{aligned} \quad (8)$$

in which $\langle a, b \rangle$ is a function that stands for the larger of the quantify a or b , $A/P| = \langle 0, (1-0,1/P)^5 \rangle$ is the Power-Law scheme employed to obtain spatial derivatives (Patankar, 1980), and $P = F/D$ is the cell Peclet number.

2.2. Discretization for trapezoidal volumes

This work uses marker particles to identify the intersection of the interfacial function, $f(x)$, which defines the solid boundary, with the Cartesian fixed grid. Marker particles have been used for more than four decades (Peskin, 1977), and are attractive due to their ability to model interfaces with complex topologies. A detailed presentation of Eulerian-Lagrangian method used in this study can be found in Udaykumar *et al.* (1996), Shyy *et al.* (1996), Udaykumar (1997), Ye *et al.* (1999) and Mariani and Prata (2008). The trapezoidal volumes in the interface between solid and fluid in the triangular cavity showed in Fig. 1, are used in the discretization of the governing equations, such volumes are presented in Fig. 3.

The integration of Eq. (4) over an interfacial control volume, such as presented in Fig. 3a, yields

$$\int_s^{n,nw} \int_l^e \frac{\partial(\rho u \phi)}{\partial x} dx dy + \int_l^s \int_s^{n,nw} \frac{\partial(\rho v \phi)}{\partial y} dy dx = \int_s^{n,nw} \int_l^e \Gamma^\phi \frac{\partial^2 \phi}{\partial x^2} dx dy + \int_l^s \int_s^{n,nw} \Gamma^\phi \frac{\partial^2 \phi}{\partial y^2} dy dx + \bar{S}^\phi. \quad (9)$$

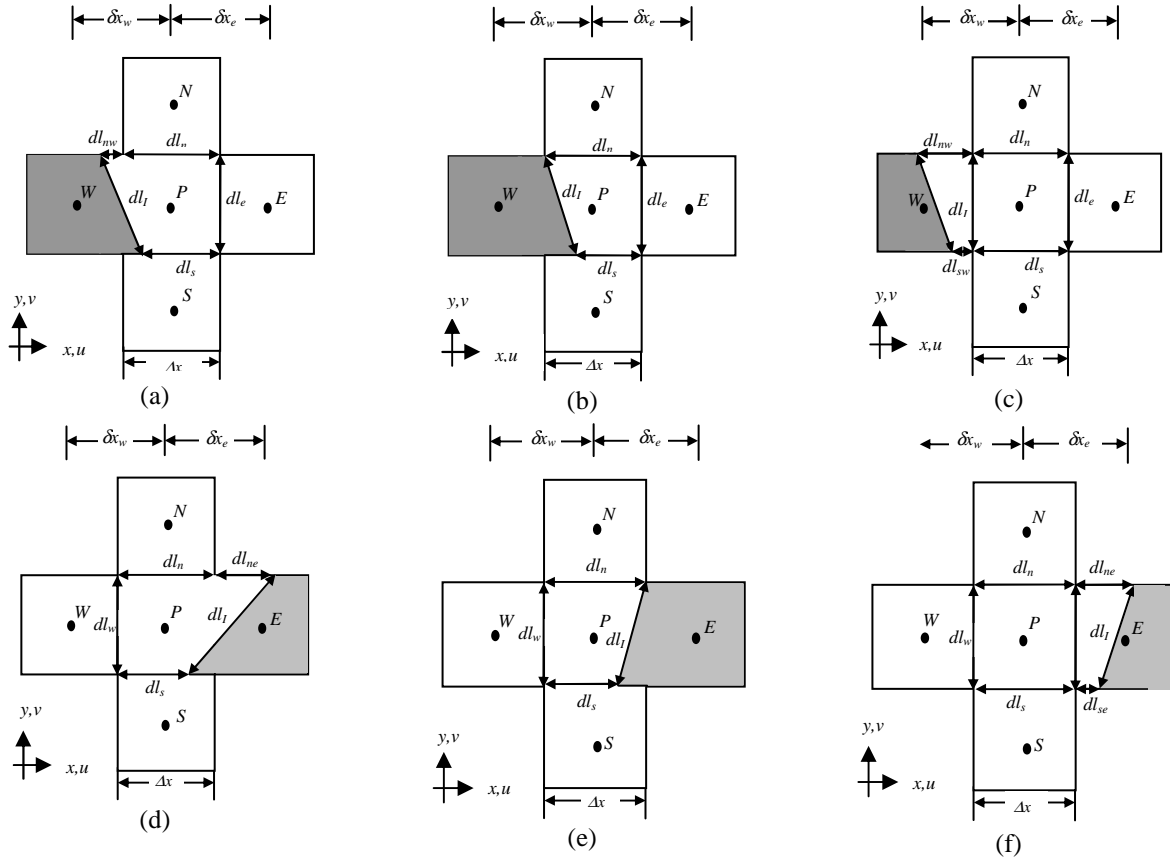


Figure 3. Trapezoidal volumes (a) first, (b) second, (c) third, (d) fourth, (e) fifth, and (f) sixth types.

After of integration of the Eq. (9) yields, for example, for the volume 1 showed in Fig. 3a, the following expression,

$$(\rho u \phi)_e dl_e - (\rho u \phi)_I dl_I + (\rho v \phi)_n dl_n + (\rho v \phi)_{nw} dl_{nw} - (\rho v \phi)_s dl_s = \bar{S}^\phi + \left(\Gamma_e^\phi \frac{\partial \phi}{\partial x} \right)_e dl_e - \left(\Gamma_I^\phi \frac{\partial \phi}{\partial n} \right)_I dl_I + \left(\Gamma_n^\phi \frac{\partial \phi}{\partial y} \right)_n dl_n + \left(\Gamma_{nw}^\phi \frac{\partial \phi}{\partial y} \right)_{nw} dl_{nw} - \left(\Gamma_s^\phi \frac{\partial \phi}{\partial y} \right)_s dl_s, \quad (10)$$

where $\bar{S}^\phi = -p_e dl_e + p_I dl_I n_x$ for $\phi = u$, or $\bar{S}^\phi = -p_n dl_n - p_{nw} dl_{nw} + p_s dl_s n_y$ for $\phi = v$. Replacing the convective fluxes and then subtracting from the resulting equation the discretized continuity equation multiplied by ϕ_P yields the following equation:

$$F_e(\phi_e - \phi_P) - F_I(\phi_I - \phi_P) + F_n(\phi_n - \phi_P) + F_{nw}(\phi_{nw} - \phi_P) - F_s(\phi_s - \phi_P) = \bar{S}^\phi + \left(\Gamma_e^\phi \frac{\partial \phi}{\partial x} \right)_e dl_e - \left(\Gamma_I^\phi \frac{\partial \phi}{\partial n} \right)_I dl_I + \left(\Gamma_n^\phi \frac{\partial \phi}{\partial y} \right)_n dl_n + \left(\Gamma_{nw}^\phi \frac{\partial \phi}{\partial y} \right)_{nw} dl_{nw} - \left(\Gamma_s^\phi \frac{\partial \phi}{\partial y} \right)_s dl_s. \quad (11)$$

The convective fluxes in interface, $u_{nI} = u_I \hat{n}_x$ for the u velocity, and $u_{nI} = u_I \hat{n}_y$ for v velocity, where \hat{n}_x and \hat{n}_y are the components of unitary vector normal to interface, in this study are nulls. Making use of total flux the Eq. (11) can be written as

$$(J_e - F_e \phi_P) + (J_n - F_n \phi_P) = \bar{S}^\phi - (J_{nw} - F_{nw} \phi_P) + (J_s - F_s \phi_P) - \left(\Gamma_I^\phi \frac{\partial \phi}{\partial n} \right)_I dl_I, \quad (12)$$

or,

$$\begin{aligned} a_P \phi_P &= a_E \phi_E + a_N \phi_N + b^\phi, \\ a_E &= D_e A(|P_e|) + \langle -F_e, 0 \rangle, \\ a_N &= D_n A(|P_n|) + \langle -F_n, 0 \rangle, \end{aligned} \quad (13)$$

$$a_p = a_E + a_N,$$

$$b^\phi = \bar{S}^\phi - (J_{nw} - F_{nw}\phi_p) + (J_s - F_s\phi_p) - \Gamma_I^\phi \frac{\partial\phi}{\partial n} \Big|_I dl_I.$$

The flux of ϕ in the solid-fluid interface can be decomposed as $(\partial\phi/\partial n)_I = (\partial\phi/\partial x)_I \hat{n}_x + (\partial\phi/\partial y)_I \hat{n}_y$, requiring computation of $\partial\phi/\partial y)_I$ (see Fig. 5) and $\partial\phi/\partial x)_I$ (see Fig. 4b) at the center of the interfacial line segment. For the cell in question (Fig. 3a), $\partial\phi/\partial x)_I$ is computed expressing the ϕ variation along the vertical line in terms of a function that is quadratic in x , for more details see the points used in Fig. 4b. The variables, ϕ_{nw} , $\partial\phi/\partial y)_{nw}$, ϕ_s , $\partial\phi/\partial y)_s$ are computed using a function that is quadratic in x and linear in y , in conformity with Ye *et al.* (1999), Mariani (2002) and Mariani and Prata (2008), see the Fig. 4a for more details.

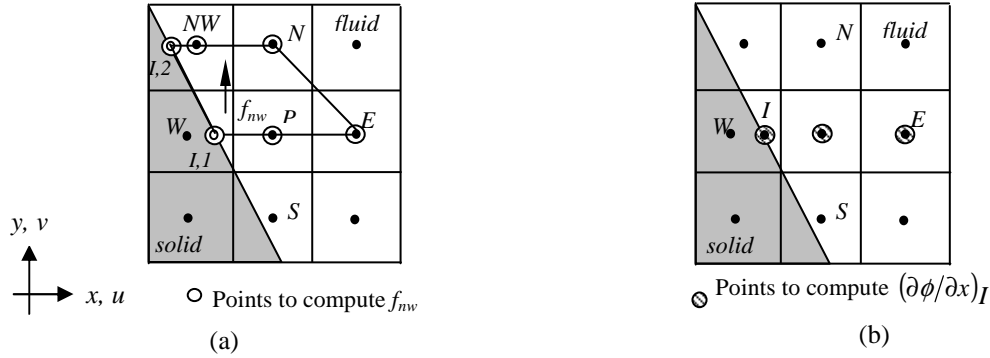


Figure 4. Points used in computation of (a) f_{nw} e (b) $(\partial\phi/\partial x)_I$.

The flux at the northwest face, nw , of control volume depicted in Fig. 3a, is approximated expressing ϕ as,

$$\phi_{nw} = c_1 x_{nw}^2 y_{nw} + c_2 x_{nw}^2 + c_3 x_{nw} y_{nw} + c_4 x_{nw} + c_5 y_{nw} + c_6,$$

$$(\partial\phi/\partial y)_{nw} = c_1 x_{nw}^2 + c_3 x_{nw} + c_5,$$
(14)

where each of the unknown coefficients, c_1 to c_6 , are expressed in terms of the values of ϕ at the six grid points shown in Fig. 4a and described as

$$\begin{cases} \phi_{I,1} = c_1 y_{I,1} x_{I,1}^2 + c_2 x_{I,1}^2 + c_3 y_{I,1} x_{I,1} + c_4 x_{I,1} + c_5 y_{I,1} + c_6 \\ \phi_P = c_1 y_P x_P^2 + c_2 x_P^2 + c_3 y_P x_P + c_4 x_P + c_5 y_P + c_6 \\ \phi_E = c_1 y_E x_E^2 + c_2 x_E^2 + c_3 y_E x_E + c_4 x_E + c_5 y_E + c_6 \\ \phi_N = c_1 y_N x_N^2 + c_2 x_N^2 + c_3 y_N x_N + c_4 x_N + c_5 y_N + c_6 \\ \phi_{NW} = c_1 y_{NW} x_{NW}^2 + c_2 x_{NW}^2 + c_3 y_{NW} x_{NW} + c_4 x_{NW} + c_5 y_{NW} + c_6 \\ \phi_{I,2} = c_1 y_{I,2} x_{I,2}^2 + c_2 x_{I,2}^2 + c_3 y_{I,2} x_{I,2} + c_4 x_{I,2} + c_5 y_{I,2} + c_6 \end{cases}.$$
(15)

The equation system shown in Eq. (15) is solved through of a direct method with partial pivoting. A similar interpolation is also used to determine f_s in south face of control volume depicted in Fig. 3a. The fluxes f_n and f_e doesn't need of special treatment because its faces weren't intercepted by interfacial function. In general, there are also interfacial volumes which have a east and west face-cut cell. To evaluate the face flux of those volumes, the interpolation function employed is linear in x and quadratic in y . For the coupling between pressure and velocity, the SIMPLEC (*Semi Implicit Method for Pressure Linked Equations Consistent*) algorithm was employed. Discretized equations are solved iteratively using the line-by-line method presented by Patankar (1980). Under-relaxation factors were employed to obtain stable convergence for the solution of mass and movement equations.

Similar to Eq. (13) can be obtained

$$a_p \phi_p = a_E \phi_E + a_W \phi_W + a_N \phi_N + a_S \phi_S + b^\phi$$
(16)

for the control volumes described in Fig. 3. The coefficients, a_p , a_E , a_W , a_N , a_S and b^ϕ are organized in Tabs. 1 to 3, including the first volume, which discretization already was described in this section.

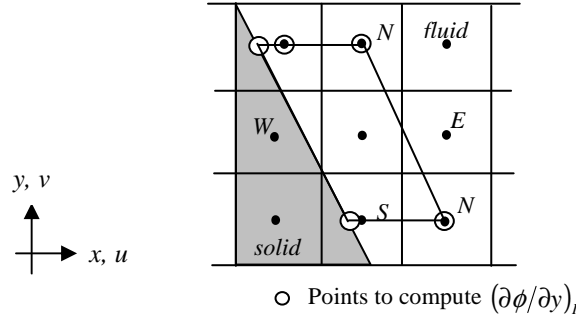


Figure 5. Points to compute $(\partial\phi/\partial y)_I$.

Table 1. Coefficients for Eq. (16).

Volume	a_p	a_E	a_W	a_N	a_S
First	$a_E + a_N$	$D_e A(P_e) + \langle -F_e, 0 \rangle$	0	$D_n A(P_n) + \langle -F_n, 0 \rangle$	0
Second	a_E	$D_e A(P_e) + \langle -F_e, 0 \rangle$	0	0	0
Third	$a_E + a_N + a_S$	$D_e A(P_e) + \langle -F_e, 0 \rangle$	0	$D_n A(P_n) + \langle -F_n, 0 \rangle$	$D_s A(P_s) + \langle F_s, 0 \rangle$
Fourth	$a_W + a_N$	0	$D_w A(P_w) + \langle F_w, 0 \rangle$	$D_n A(P_n) + \langle -F_n, 0 \rangle$	0
Fifth	a_W	0	$D_w A(P_w) + \langle F_w, 0 \rangle$	0	0
Sixth	$a_W + a_N + a_S$	0	$D_w A(P_w) + \langle F_w, 0 \rangle$	$D_n A(P_n) + \langle -F_n, 0 \rangle$	$D_s A(P_s) + \langle F_s, 0 \rangle$

Table 2. Source term, total and convective fluxes used in Tab. 1.

Volume	b^ϕ	J	F
First	$\bar{S}^\phi - (J_{nw} - F_{nw}\phi_p) + (J_s - F_s\phi_p) - \Gamma_I^\phi \frac{\partial\phi}{\partial n} \Big _I dl_I$	$F_n\phi_n - \Gamma_n^\phi \frac{\partial\phi}{\partial y} \Big _n dl_n$	$\rho v dl \Big _n$
Second	$\bar{S}^\phi - \Gamma_I^\phi \frac{\partial\phi}{\partial n} \Big _I dl_I - (J_n - F_n\phi_p) + (J_s - F_s\phi_p)$	$F_{ne}\phi_{ne} - \Gamma_{ne}^\phi \frac{\partial\phi}{\partial y} \Big _{ne} dl_{ne}$	$\rho v dl \Big _{ne}$
Third	$\bar{S}^\phi - (J_{nw} - F_{nw}\phi_p) + (J_{sw} - F_{sw}\phi_p) - \Gamma_I^\phi \frac{\partial\phi}{\partial n} \Big _I dl_I$	$F_{nw}\phi_{nw} - \Gamma_{nw}^\phi \frac{\partial\phi}{\partial y} \Big _{nw} dl_{nw}$	$\rho v dl \Big _{nw}$
Fourth	$\bar{S}^\phi - (J_{ne} - F_{ne}\phi_p) + (J_s - F_s\phi_p) + \Gamma_I^\phi \frac{\partial\phi}{\partial n} \Big _I dl_I$	$-F_s\phi_s + \Gamma_s^\phi \frac{\partial\phi}{\partial y} \Big _s dl_s$	$\rho v dl \Big _s$
Fifth	$\bar{S}^\phi + \Gamma_I^\phi \frac{\partial\phi}{\partial n} \Big _I dl_I - (J_n - F_n\phi_p) + (J_s - F_s\phi_p)$	$-F_{se}\phi_{se} + \Gamma_{se}^\phi \frac{\partial\phi}{\partial y} \Big _{se} dl_{se}$	$\rho v dl \Big _{se}$
Sixth	$\bar{S}^\phi - (J_{ne} - F_{ne}\phi_p) + (J_{se} - F_{se}\phi_p) - \Gamma_I^\phi \frac{\partial\phi}{\partial n} \Big _I dl_I$	$-F_{sw}\phi_{sw} + \Gamma_{sw}^\phi \frac{\partial\phi}{\partial y} \Big _{sw} dl_{sw}$	$\rho v dl \Big _{sw}$

Table 3. Variable ϕ and $(\partial\phi/\partial y)$.

Faces	ϕ	$(\partial\phi/\partial y)$
n	$c_1 x_n^2 y_n + c_2 x_n^2 + c_3 x_n y_n + c_4 x_n + c_5 y_n + c_6$	$c_1 x_n^2 + c_3 x_n + c_5$
ne	$c_1 x_{ne}^2 y_{ne} + c_2 x_{ne}^2 + c_3 x_{ne} y_{ne} + c_4 x_{ne} + c_5 y_{ne} + c_6$	$c_1 x_{ne}^2 + c_3 x_{ne} + c_5$
nw	$c_1 x_{nw}^2 y_{nw} + c_2 x_{nw}^2 + c_3 x_{nw} y_{nw} + c_4 x_{nw} + c_5 y_{nw} + c_6$	$c_1 x_{nw}^2 + c_3 x_{nw} + c_5$
s	$c_1 x_s^2 y_s + c_2 x_s^2 + c_3 x_s y_s + c_4 x_s + c_5 y_s + c_6$	$c_1 x_s^2 + c_3 x_s + c_5$
se	$c_1 x_{se}^2 y_{se} + c_2 x_{se}^2 + c_3 x_{se} y_{se} + c_4 x_{se} + c_5 y_{se} + c_6$	$c_1 x_{se}^2 + c_3 x_{se} + c_5$
sw	$c_1 x_{sw}^2 y_{sw} + c_2 x_{sw}^2 + c_3 x_{sw} y_{sw} + c_4 x_{sw} + c_5 y_{sw} + c_6$	$c_1 x_{sw}^2 + c_3 x_{sw} + c_5$

3. NUMERICAL RESULTS

In this section is presented flow patterns and characteristic parameters for a triangular cavity with different Reynolds numbers. Numerical tests for a variety of triangular geometries have been investigated, but for brevity, only give here the description for the equilateral cavity. Using meshes 30×60, 60×120, 120×240, and 240×480, we obtain numerical results for a Reynolds number up to 1. The comparison between the coarse and fine grids in terms of accuracy of numerical results and computational time show the reliability using a coarse grid, formed by 120×240 control volumes. Detailed characteristics parameters are given in Tab. 4. It can be seen from Tab. 4 that our results are in good agreement with those obtained by Li e Tang (1996) and McQuain et al. (1994). In that table, the stream function describe the

vector field (u, v) by a simple scalar quantity, ψ . The relation between velocity and stream function is based in mass conservation equation and can be expressed as,

$$u = \frac{1}{\rho} \frac{\partial \psi}{\partial y}, \tag{17}$$

$$v = -\frac{1}{\rho} \frac{\partial \psi}{\partial x}. \tag{18}$$

The vorticity is twice the angular velocity of air in any point, or is the measure of fluid rotation accordant it moves in flow field, is described as,

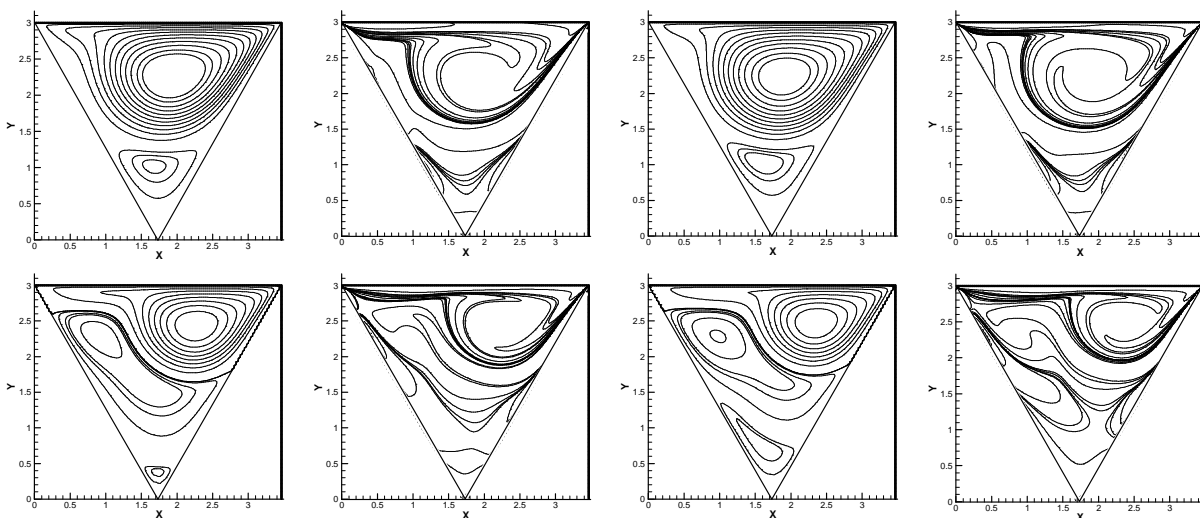
$$\zeta = \frac{\partial v}{\partial x} - \frac{\partial u}{\partial y}. \tag{19}$$

To verify the accuracy of the results presented in Tab. 4 was computed the absolute error, $|\phi_p - \phi_o|$, where the subscript p denotes the present work and the subscript o denotes the works of other authors. Comparing the values of the stream function, the biggest error was obtained to $Re = 200$, with the value of 3.3% confronted to Li and Tang (1996) and the smallest error was obtained to $Re = 1$ with the value of 0.4% compared to McQuain *et al.* (1994). For the vorticity the biggest error was obtained to $Re = 200$ with the value of 2.69% compared to Li and Tang (1996) and smallest error was obtained to $Re = 1$ with the value of 0.5% confronting to Li and Tang (1996). The order of the errors obtained shown that the method employed in the present work is acceptable to solve the flow in the triangular cavity with reasonable accuracy.

The streamlines and contours of the vorticity are depicted in Fig. 6 shown the standard of flow with the increasing of Reynolds number since 1,000 to 6,000. The topmost eddy deviates from this sequence with increase in Reynolds number, since inertial effects near the top wall become more important as Re increases. All figures show similar eddies of decreasing size towards the lower corner of the cavity. For all Reynolds numbers, the lower eddy has their centers along the centerline of the cavity. The topmost eddy, where inertial effects are dominant, first moves to the right as Re increases and later moves back towards the center of the cavity, while the second eddy moves to the left and increases with the Reynolds number. Plots of the contours of constant vorticity are shown in Fig. 6 for $Re = 1,000$ to 6,000. It is seen that for small Re , the vorticity field is symmetrical about the centerline. However, as Re increases, the vorticity variation moves to the boundary regions of the cavity, while the interior or the topmost eddy tends to attain constant vorticity.

Table 4. Properties of the center of the primary eddy, located at (x, y) with stream function value ψ and vorticity ζ .

Re	Source	ψ	ζ	x	y
1	Present work	0.229	1.373	1.732	2.475
	Li and Tang (1996)	0.235	1.368	1.767	2.460
	McQuain <i>et al.</i> (1994)	0.233	1.363	1.749	2.460
200	Present work	0.236	1.481	2.107	2.438
	Li and Tang (1996)	0.269	1.212	1.940	2.280
	McQuain <i>et al.</i> (1994)	0.260	1.272	1.940	2.280
500	Present work	0.247	1.321	2.021	2.325
	Li and Tang (1996)	0.279	1.066	1.871	2.160
	McQuain <i>et al.</i> (1994)	0.269	1.250	1.905	2.265



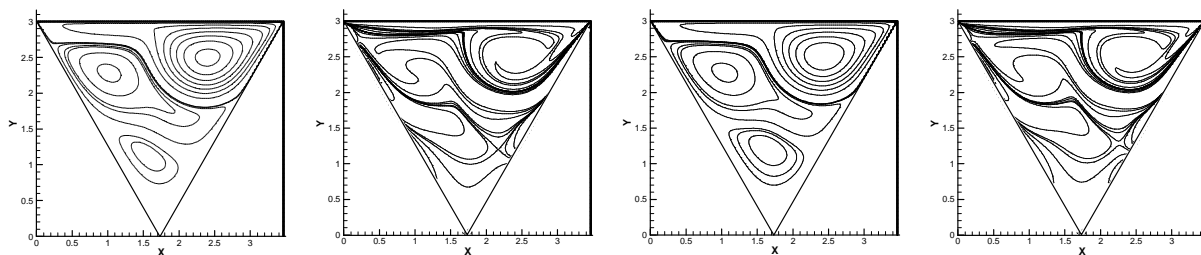


Figure 6. Streamlines and contours of the vorticity, respectively, for $Re = 1,000; 2,000; 3,000; 4,000; 5,000$ and $6,000$.

4. CONCLUSIONS

In this paper was presented the results of a steady viscous flow simulation in a triangular cavity. With the use of Cartesian grids and an Eulerian-Lagrangian method, the solution was obtained without encountering any difficulties. The present approach proved to be quite successful and yielded accurate solutions for high Reynolds numbers. The numerical results obtained in this study were compared with results reported in literature and the agreement is good.

5. ACKNOWLEDGMENTS

The present work was developed with financial support of Fundação Araucária (FA 44/07 P9130), and the first author thanks scholarship received by Pontifical Catholic University of Paraná.

6. REFERENCES

- BATCHELOR, G. K., 1956, On steady laminar flow with closed streamlines at large Reynolds number, *Journal of Fluid Mechanics*, Vol. 1, pp. 177-190.
- DARR, J. H. & VANKA, S. P., 1991, Separated flow in a driven trapezoidal cavity, *Physics of Fluids, A*, Vol. 3, pp. 385-392.
- FOX, R. W., & MCDONALD, A. T., 2001, *Introdução à Mecânica dos Fluidos*, 5^a. ed., Rio de Janeiro: LTC, 662 p.
- GLOWINSKI, R., GUIDOBONI, G., & PAN, T.-W., 2006, Wall-driven incompressible viscous flow in a two-dimensional semi-circular cavity, *Journal of Computational Physics*, 216, pp. 76-91.
- JYOTSNA, R., & VANKA, P., 1995, Multigrid Calculation of Steady, Viscous Flow in a Triangular Cavity, *Journal of Computational Physics*, 122, pp.107-117.
- LI, M., & TANG, T., 1996, Steady Viscous Flow in a Triangular cavity by Efficient Numerical Techniques, *Computers Mathematical Applic.*, 31, pp. 55-65.
- MARIANI, V. C., 2002, *Métodos de otimização e técnicas de modelagem de interface para análise de escoamento de fluidos em difusores radiais com geometrias irregulares*, Tese de Doutorado defendida no Departamento de Engenharia Mecânica, Universidade Federal de Santa Catarina, Brasil, 331 p.
- MARIANI V. C. & PRATA A. T., 2008, A Eulerian-Lagrangian Method Applied to Fluid Flow in Lid-Driven Cavities With Irregular Bottom Walls, *Numerical Heat Transfer*, Vol. 53, pp. 206-233.
- MCQUAIN, W. D., RIBBENS, C. J., WANG, C.-Y. & WATSON, L.T., 1994, Steady viscous flow in a trapezoidal cavity, *Computers & Fluids*, 23, pp. 613-626.
- MOFFAT, H. K., 1963, Viscous and resistive eddies near a sharp corner, *Journal of Fluid Mechanics*, Vol. 18, pp. 1-18.
- PATANKAR, S. V., 1980, *Numerical Heat Transfer and Fluid Flow*, McGraw-Hill.
- PESKIN, C. S., 1977, Numerical-Analysis of Blood-Flow in Heart, *Journal of Computational Physics*, Vol. 25, pp. 220-252.
- RIBBENS, C. J., WANG, C. -Y., WATSON, L. T. & ALEXANDER, K. A., 1991, Vorticity induced by a moving elliptic belt, *Computers & Fluids*, Vol. 20, pp. 111-119
- RIBBENS, C. J., WATSON, L. T. & WANG, C. -Y., J. 1994, Steady viscous flow in a triangular cavity, *Journal of Computational Physics*, Vol. 112, pp. 173-181.
- SHYY, W., UDAYKUMAR, H. S., RAO, M. M. & SMITH, R. W., 1996, *Computational Fluid Dynamics with Moving Boundaries*, Taylor & Francis, Bristol, PA.
- UDAYKUMAR, H. S., SHYY W. & RAO, M. M., 1996, ELAFINT: A Mixed Eulerian-Lagrangian Method for Fluid Flows with Complex and Moving Boundaries, *International Journal for Numerical Methods in Fluids*, Vol. 22, pp. 691-712.
- UDAYKUMAR, H. S., KAN, H.-C., SHYY, W. & TAY-SON-TRAN, R., 1997, Multiphase Dynamics in Arbitrary Geometries on Fixed Cartesian Grids, *Journal of Computational Physics*, Vol. 137, pp. 366-405, 1997.
- VYNNYCKY, M. & KIMURA, S., 1994, An investigation of recirculating in a driven cavity, *Physics of Fluids, A*, Vol. 6, pp. 3610-3620.
- YE, T., MITTAL, R., UDAYKUMAR, H. S., & W. SHYY, A Cartesian Grid Method for Viscous Incompressible Flows with Complex Immersed Boundaries, *37th AIAA Aerospace Sciences Meeting and Exhibit*, Reno, NV, 1999.